LRP 479/93 July 1993

TIME-RESOLVED MEASUREMENTS OF HIGHLY-POLYMERISED NEGATIVE IONS IN RF SILANE PLASMA DEPOSITION EXPERIMENTS

A.A. Howling, L. Sansonnens, J.-L. Dorier & Ch. Hollenstein

submitted to J. Appl. Phys. 19 July 1993

Time-resolved measurements of highly-polymerised negative ions in rf silane plasma deposition experiments

A. A. Howling, L. Sansonnens, J.-L. Dorier and Ch. Hollenstein

Centre de Recherches en Physique des Plasmas,

Ecole Polytechnique Fédérale de Lausanne,

Av. des Bains 21, CH-1007 Lausanne, Switzerland

ABSTRACT

The time-resolved fluxes of negative polysilicon hydride ions from a power-modulated rf silane plasma have been measured by quadrupole mass spectrometry and modeled using a simple polymerisation scheme. Experiments were performed with plasma parameters suitable for high-quality amorphous silicon deposition. Polysilicon hydride anions diffuse from the plasma with low energy (approximately 0.5 eV) during the afterglow after the electron density has decayed and the sheath fields have collapsed. The mass-dependence of the temporal behavior of the anion loss flux demonstrates that the plasma composition is influenced by the modulation frequency. The negative species attain much higher masses than the positive or neutral species, and anions containing as many as sixteen silicon atoms have been observed, corresponding to the 500 amu limit of the mass spectrometer. This suggests that negative ions could be the precursors to particle formation. Ion-molecule and ion-ion reactions are discussed and a simple negative ion polymerisation scheme is proposed which qualitatively reproduces the experimental results. The model shows that the densities of high mass negative ions in the plasma are strongly reduced by modulation frequencies near 1 kHz. Each plasma period is then too short for the polymerisation chain to propagate to high masses before the elementary anions are lost in each subsequent afterglow period. This explains why modulation of the rf power can reduce particle contamination. We conclude that, for the case of silane rf plasmas, the initiation steps which ultimately lead to particle contamination proceed by negative ion polymerisation.

PACS numbers : 52.80.Hc, 52.80.Pi, 82.80.Ms, 82.40.Ra

I. INTRODUCTION

Plasma deposition of amorphous silicon (a-Si:H) is particularly suited to large area electronics for optical imaging devices, matrix-addressed arrays and solar cells, to name just a few commercial applications. However, it has become clear that particulate contamination presents a major problem by limiting manufacturing productivity and device reliability. Modern trends towards larger circuit dimensions together with smaller feature size and higher component densities will aggravate the risk of particle-related yield losses, for example, a single defect on a matrix array could mean the loss of the entire display whereas a defect on a silicon wafer may damage only one of many separate devices.

Selwyn and co-workers[1-3] have shown that particles created during the plasma are the major contributors to wafer contamination. Indeed, a condition for the deposition of device quality amorphous silicon can be empirically defined as an absence of plasma polymerisation and particle formation. Particles form in plasmas used for deposition,[4] etching[1] and sputtering,[3,5] where they can be detected in situ by light scattering.[2,6-9] Power modulation strongly diminishes powder formation in rf silane plasmas[4,8,10,11] and has been shown to be beneficial for film quality.[4,10,12,13] This technique is further investigated in this paper.

The maximum achievable deposition rate for device quality intrinsic a-Si:H is limited by plasma polymerisation which results in poorer electronic properties[14,15] and rough films.[16] The density of particles occluded in the film has been found to rise with increasing deposition rate, no matter how this increase is obtained.[16,17] Conventionally, 'polymerisation' involves the synthesis of chains of repeated molecular units called monomers, but in 'plasma state polymerisation', the primary process depends on energetic electrons to dissociate the feed gas, allowing the formation of unconventional materials. Strictly, 'polymer' (for the resultant film) and 'monomer' (for the feed gas) are misnomers since there is no repetition of a unique unit along a polymer chain.[16-18]

The initiation step of plasma polymerisation can be investigated using plasma diagnostics to provide information on the identity of the precursor species which can be neutral, positive, negative, or a combination of these. It may well be that there is no unique pathway for

producing powder from silane and that different conditions favor different species.[18] This paper concentrates on the technologically-important process of rf silane plasmas with parameters suitable for high-quality a-Si:H deposition since the species responsible for the initial polymerisation pathway have still not been identified.[19]

Neutral radicals are candidates for particle precursors and propagation is supposed to be by insertion of lower silane radicals into higher saturated molecules.[20,21] However, the largest polysilane neutrals reported are trisilane for rf discharges[22] and pentasilane in dc discharges.[21] Thermal dissociation of silane by a filament at 1500 °C does produce much heavier neutral clusters[23] without depending on any ionic pathway.[21]

Plasma polymerisation is expected to be more rapid for ions. Positive ions in silane-containing plasmas[22,24] have been invoked as particle precursors in several models,[20,25,26] although experiments by Mandich *et al* [19] show that activation energy barriers occur which prevent the formation of high mass positive ions. Certain plasma conditions can nevertheless overcome these energy barriers and lead to very high mass positive ionic clusters.[23]

The fact that negative ions are retained in the plasma by the sheath potentials has led several authors to suggest that plasma polymerisation might proceed via negative ion pathways.[10,12,27-29] Negative ions in silane plasmas were first reported by Perrin *et al* [27] in a multipole source and other authors have also shown that several positive and negative species co-exist in other plasmas[30] where negative ions can be the heaviest species.[31] We have since detected negative ions up to mass 500 amu in rf silane plasmas[32] and have also shown an anti-correlation between negative ion loss and powder formation in modulated silane plasmas.[33]

Electronegative gases have wide commercial use for plasma etching and deposition and so it is desirable to know the identity of the negative ions, their influence on the plasma chemistry, powder formation and the growing film, and how they can be controlled and exploited to improve existing processes. Negative ions formed by electric discharges are generally very reactive but because of the technical difficulties associated with their detection, the role of negative ions has however only rarely been seriously considered.[18] Both rf plasma simulations[34] and experiments[35-37] show that negative ion densities in halogen-containing gases can reach densities of one or two orders of magnitude greater than the free electron

densities, and the addition of only a few percent of an electronegative gas to a noble gas plasma can strongly reduce the free electron density.[38] Negative ion kinetics also influence rf discharges by forming double layers, as determined experimentally[39,40] and by simulation.[41,42] The importance of negative ions in determining plasma properties is therefore clear. Silane, however, is weakly electronegative compared to halogen gases and has received little attention regarding negative ions, although the research which has been done finds significant densities.[10,27,38,43-46]

Negative ions have been previously investigated by two-photon laser-induced fluorescence,[1] optogalvanic effects,[35,39] microwave interferometry[46,47] and micowave cavity techniques[38] combined with photodetachment.[36,37,48] Langmuir probes, reviewed by Amemiya,[49] can also be used for negative ion measurements. Mass spectrometry, using quadrupole mass filters,[27,30-33,50,51] Fourier transform,[52,53] crossed beam[54] or time-of-flight methods,[55] is the only diagnostic technique capable of establishing the composition of complex negative molecular ion groups.

In this paper we use quadrupole mass spectrometry to measure the time-resolved diffusion of heavy polymerised negative ions from power-modulated rf silane plasmas. There are several difficulties associated with mass spectrometry of negative cluster ions in time-varying deposition plasmas[10,56] and therefore the first part of the experimental results in Section III is intended to show that the measurements presented here are viable. The results are interpreted following the model of Overzet *et al* [31], and a simple polymerisation scheme is proposed to demonstrate the effect of modulation frequency on particle formation in silane plasmas.

II. EXPERIMENTAL METHOD

The experimental apparatus shown in Fig. 1 is a conventional parallel-plate rf capacitive reactor comprising two 130 mm diameter electrodes with a 25 mm electrode gap and a grounded guard screen on the lower, rf electrode. The gas inlet is in the side wall of the cubic steel vacuum chamber of side 400 mm. Plasma parameters which gave good quality a-Si:H films were chosen, namely, a 30 sccm pure silane flow at 0.1 mbar pressure. The silane

depletion, estimated by mass spectrometry, was not more than 10 %. The substrate temperature on the upper, grounded electrode was 150 °C and the rf electrode and the grounded chamber walls were maintained at 80 °C. Base pressures of 10^{-7} mbar were routinely obtained.

The rf power was on/off modulated by mixing a low frequency (10 Hz to 20 kHz) square wave into the rf generator signal using a Hewlett-Packard 10534A balanced mixer before amplification by an RF Power Labs wideband (10 kHz - 200 MHz) amplifier. The rf power, at an excitation frequency of 30 MHz, was capacitively-coupled to the rf electrode via a rf power meter and a π matching network. The peak-to-peak voltage for all of these experiments was 115 V to within ± 5 V (neglecting transient peaks at the beginning of each plasma period) and the rise- and fall-time of the electrode voltage was 0.2 μs. This was measured directly at the underside of the rf electrode with a passive rf voltage probe which we used to estimate a time-averaged plasma power of 4 W,[57] corresponding to 8 W during the plasma half-cycle. During the plasma period, the surface-averaged power density was therefore 60 $mWcm^{-2}$ (24 $mWcm^{-3}$ volume-averaged). The mass spectrometer electronics were immune to rf interference for these rf power levels. The rf electrode self-bias was about -25 V, showing that its area is less than the effective grounded electrode surface as regards plasma current flow.[58] This is to be expected from the reactor geometry in Fig.1 although the plasma visible emission was well-confined in the electrode gap. Identical plasma conditions were employed for all the work presented in this paper, with modulation frequency being the only variable parameter.

The differentially-pumped mass spectrometer was a Hiden Analytical Limited Plasma Monitor[59] type HAL-EQP 500 for masses 1-500 amu, shown to scale in Fig. 1. The grounded ion extractor head was positioned with its axis in the electrode plane 10 mm beyond the grounded guard screen, separate from the well-confined glow region. In this work, therefore, ions were not extracted at the grounded electrode but at the mass spectrometer head which was at the same potential. The rf electrode voltage and plasma emission axial symmetry were unaffected by insertion of the monitor to this position.

Single-stage differential pumping maintained an operational pressure in the monitor of 10^{-6} mbar and so the ions would reach the detector with negligible probability of secondary

reactions with the residual gas. Ions entered the monitor first through a 5 mm diameter orifice in the spectrometer head and then a 100 μm aperture in the biased extractor electrode. A +40 V bias on the extraction electrode gave a good negative ion signal without creating a visible secondary plasma in the extraction orifice. No dc bias on the rf plasma electrode was necessary to detect negative ions unlike other experiments[31,50] where negative ions were collected at the grounded plasma electrode. The positive ion intensity did not depend strongly on the negative extraction bias voltage as expected, and a -150 V bias was used for this work.

Following extraction, the ions were accelerated into a drift tube followed by a 45° electrostatic energy analyser selecting an ion energy of 42.4 eV in our case. The energy analyser half-width resolution of about ± 1.5 eV was not optimised in order to maintain a high transmission efficiency, and a possible systematic error of ± 0.5 eV on the energy value may also exist due to field penetration effects at the monitor electrodes. Ions then passed through a quadrupole mass filter and were detected by a channeltron. For time-resolved measurements, the channeltron pulses triggered by individual ion events were registered by a gated counter (referenced to the square-wave signal generator) with a time window of 5 μs integrating over 10'000 power modulation cycles.

The transit time of an ion crossing the spectrometer introduces a non-negligible mass-dependent 'instrumental delay' with respect to the power modulation timing. The transit times for different molecular ions were estimated empirically from the onset time for the positive ion signal and from the negative ion 'cut-off' time when the plasma period restarts and are compared with calculation in Figure 2. The transit times were thus calibrated to ± 3 μs, and have been implicitly subtracted from all the time-resolved data presented in this work .

One of the principal difficulties of mass spectrometry in deposition plasmas is that the deposited film or powder can block the aperture,[10] or at least alter the ion extractor electric field by electrostatic charging of the accumulated deposition on its surface.[56] Any such modification to the ion extraction field was detectable by monitoring changes in the ion intensity as a function of extraction voltage. The monitor extraction head was dismantled and cleaned in acid after every few hours of exposure to the plasma.

III. RESULTS

A. Mechanism of negative ion extraction

Mass spectrometry cannot be used to measure negative ions in continuous silane plasmas because they are trapped within the discharge volume by sheath potentials which arise to prevent the escape of high-mobility electrons. The existence of negative silane ions in continuous plasmas has been proven by other methods.[38,45,46]

In power-modulated plasmas, provided that the modulation depth is at least 90 %,[50] the sheaths collapse sufficiently for negative ions to escape if the afterglow period is long enough. Figure 3 shows the time-dependence of ion fluxes to the plasma monitor at a 2 kHz modulation frequency where we have taken the $Si_2H_5^+$ and $Si_2H_5^-$ ions, measured separately, as examples. Also shown is the SiH* emission at 414 nm using a spectrometer and gated optical multichannel analyser with a 1 μs time window. Figure 4 shows the corresponding time-averaged energy spectra for both ions.

We can interpret the mechanism of positive and negative ion loss from the plasma using Figures 3 and 4 :

When the electrode voltage is applied at the beginning of each cycle, energetic electrons (at least 8 eV) are created which dissociate silane and give rise to a sharp SiH* emission peak in less than 2 μs. Equilibrium between the power source and the various plasma species is established on a slower timescale of around 30 μs. $Si_2H_5^+$ ions formed in the plasma are accelerated across the sheaths and reach the grounded monitor surface with approximately 30 eV maximum (Fig. 4), which implies a time-averaged plasma potential of +30 V (ions can only respond to potentials averaged over many rf cycles for this high excitation frequency[58]). Ions with less than 30 eV have lost energy in inelastic collisions in crossing the sheath, or were formed by ionisation or charge-exchange within the sheath; some low energy ion contribution may also come from ions in the afterglow period.

In Fig. 3, when the rf power is removed at 250 μs, the most energetic electrons rapidly leave the plasma and the SiH* emission completely disappears in 4 μs. Thereafter, positive ions and electrons undergo ambipolar diffusion to the electrode surfaces and the positive ion

flux falls. After a delay of 110 μs from the end of the power period, the negative ion flux appears abruptly and gradually decays until the next power period starts when the flux is cut off by the sheath formation. Delays in the onset of negative ion flux have previously been observed both experimentally[36,50,56] and by simulation[29] and can be interpreted as follows : When the electron density decays during the afterglow, the negative ion density eventually becomes large compared to the electron density. The plasma potential then no longer needs to be positive to retain electrons since the mobilities of the remaining positive and negative ions are comparable, and the sheath field collpases.[39,40] An electric field then drives negative ions to the boundaries. The negative ions would be expected to leave the plasma with near-thermal energies,[29,40] and this would explain the very low negative ion energies shown in Fig. 4. The ions are singly-charged and so we deduce a plasma potential of about -0.5 V although the energy resolution and systematic errors are relatively large as described in the preceding section.

The level of perturbation of the extraction electrode bias voltage on the plasma can be gauged from Fig. 3 using the fact that the negative and positive ion fluxes should be mutually exclusive based on the above interpretation : The persistence of the negative ion signal during the plasma period and of the positive ion signal during the negative ion diffusion period is probably due to the extraction voltage locally retarding the tendency of the sheath potential to change sign. From Fig. 3, this effect overestimates the negative and positive ion signals by approximately 15 and 5 % respectively, although the error may be larger for higher modulation frequencies (see Figure 5 below). Different extraction voltages, provided they were not so high as to cause a secondary plasma in the orifice, did not affect the negative ion delay time or the ion energy distributions.

These data demonstrate that the method of measurement gives results which are consistent with simulations and other experiments. In the next section, we consider measurements of negative ion clusters as a function of modulation frequency and cluster size.

B. Time-resolved measurements of negative ion clusters

Figure 5 shows the time development of the $Si_2H_5^-$ intensities for four power modulation frequencies in plasma conditions otherwise identical to Fig. 3. The general scheme

of a delay followed by a negative ion pulse and decay is qualitatively reproduced, but the delay time and pulse amplitude are modulation frequency-dependent. Figure 6 compares the $Si_2H_5^-$ signal onset delay time with the afterglow period.

The $Si_2H_5^-$ negative ions are completely emptied from the discharge volume during the afterglow only for modulation frequencies less than about 500 Hz. At 5 kHz, the $Si_2H_5^-$ negative ion flux has only just enough time to appear before the next plasma period begins. Extrapolation of the delay time curve in Fig. 6 shows that no $Si_2H_5^-$ ions would escape from the plasma for a 15 kHz modulation frequency because then the estimated 33 μs delay time equals the afterglow period. For higher modulation frequencies the negative ions accumulate in the plasma volume during successive modulation power cycles. Note that the modulation frequency is consequently a crucial parameter for determining the $Si_2H_5^-$ negative ion loss rates and hence will directly influence their time-averaged density.

All the above results were obtained for Si_2H_5 ions using sufficient mass resolution to distinguish between ions with different numbers of hydrogen atoms.[33] The following results were all obtained with strongly-degraded resolution of the quadrupole mass filter to maximise the transmission efficiency of the spectrometer. This also has the advantage of improving the signal-to-noise ratio for negative ion operation because the background signal from stray electrons accelerated onto the channeltron is independent of the quadrupole mass resolution. Each polysilicon hydride anion signal therefore represents the combined intensities of all the negative ions having the same number of silicon atoms irrespective of their hydrogen content or isomeric structure - the relative abundance of the individual negative ion radicals within the first four groups can be found in Ref. 33.

Figure 7 shows the time-resolved behavior of mono- through to hexa-silicon hydride anions. A striking characteristic is the double peak in the monosilicon hydride anion group which also exists to a lesser extent for the di- and tri-silicon hydride anion species. The first peak follows only a few microseconds after the end of the plasma period and decays almost completely before the onset of the delayed ion flux peak. A sheath collapse mechanism cannot be responsible for these initial peaks. This observation is predicted by the model of Overzet *et al* [31] and is explained as follows : on plasma extinction, energetic electrons can cross the

decaying sheath region and some attach to neutral molecules; the resulting negative ions are formed very close to the spectrometer orifice and are therefore detected within a few microseconds of the end of the plasma period. The second peak is due to negative ions from the plasma bulk which escape when the sheath collapses, as described earlier.

Figure 7 therefore shows that 40 % of the monosilicon hydride anion flux is not due to ions existing in the active plasma whereas almost all of the heavier negative ions observed are in fact ions formed during the plasma period. Overzet *et al* [31,50] also deduced that the majority of negative ions observed in other electronegative discharges were created during the active plasma and not during the afterglow. The observation that the initial peaks of di- and tri-silicon hydride anions are smaller, and very weak for higher masses, shows either that attachment to polysilane molecules is much slower than to monosilane molecules, and/or that the density of polysilane neutrals available for attachment is much lower than the monosilane density. The latter explanation would seem to be the most reasonable and is also borne out by direct measurement of neutral radical densities as will be shown in Figure 11 below. The fact that the initial, attachment peak decays almost to zero before the delayed diffusion peak arrives is supplementary proof that the electron density falls to a very low value before the sheath collapses : Since the silane density is constant at all times, the monosilicon hydride anion initial peak represents the time-resolved convolution of the silane attachment cross-section with the electron energy distribution. Assuming to a first appoximation that this depends only on the electron density, we estimate a 1/e time constant of 36 μs for the electron density decay in the afterglow for these plasma conditions at 1 kHz modulation frequency.

Fig. 7 also shows that only the monosilicon hydride anions have enough time to completely disappear for a 1 kHz modulation frequency. Because of the mass-dependent delay times and decay time constants, the loss rates and hence negative ion densities depend on the modulation frequency in different ways according to their mass, that is, *the modulation frequency influences the composition of the plasma* . This point will be demonstrated by a simple polymerisation model in Section IVB.

Figure 8 shows the normalised time-resolved fluxes for the first four positive ion groups. Figure 9 compares the positive ion decay time constant after plasma extinction and the

delay time for the negative ion diffusion peak appearance for each mass. The data points for both ion types can be approximately described by an inverse square root mass-dependence. This suggests that the positive ion density profile collapses by ambipolar diffusion of the ions during the sheath decay, to be followed by a similar collapse of the negative ion density profile once the sheath field has reversed, although other source and loss terms are neglected in this simple description.

C. Time-averaged measurements of negative ion clusters and the dependence on modulation frequency

Figure 10 (reproduced from Ref. 32) shows the negative and positive ion mass spectra, obtained with low mass resolution, which are the time-averaged signals measured with plasma conditions and mass spectrometer settings identical to those used for Figures 7 and 8. Each peak therefore represents the combined intensities of those polysilicon ions having the same number of silicon atoms irrespective of their hydrogen content.

Negative polysilicon hydride ionic clusters were observed right up to the 500 amu mass limit of the mass spectrometer, corresponding to hexadecasilicon hydride anions $[Si_{16}H_x]^-$. Clearly, heavy negative ions do exist in this silane plasma and could conceivably be the polymerisation pathway to larger clusters and ultimately to powder particles. These negative molecular ions are singly-charged by incorporation of an electron into a molecular orbital and they do not have a sheath just in the same way that a free electron is not surrounded by a sheath. The concept of sheaths and floating potential only apply when the object is large enough so that it is statistically meaningful to speak of electron and positive ion fluxes to its surface.[28,60,61]

The mass distribution within the negative ion groups of Fig. 10 is an indicator of the cluster structure. For the first four groups, the most abundant negative ions $[Si_nH_{2n+1}]^-$ ($n \leq 4$) are isoelectronic with the equivalent saturated neutral molecule Si_nH_{2n+2}.[33] The penta- and hexa-silicon hydride anion groups appear to have a strong pure silicon component, Si_5^- and Si_6^-. Thereafter the cluster composition, although broad, has a maximum intensity for $[Si_nH_{n+p}]^-$ (where $n \geq 7$ and $p = 3 - 5$). These clusters are therefore highly cross-linked,

three-dimensional structures[17,23] whose hydrogen content lies between that of saturated molecules Si_nH_{2n+2} and amorphous silicon material (≈ 10 atomic % hydrogen).

The positive ion masses in Fig. 10 are limited to only 150 amu, corresponding to pentasiliconium ions $[Si_5H_x]^+$, possibly because the activation energy barriers described by Mandich *et al* [19] inhibit further cluster growth. The positive ion size might also be limited because of ion-ion recombination losses, or because they are efficiently evacuated from the plasma across the sheaths. The weak intermediate peaks in the positive ion spectrum are most probably due to ions of type $[Si_{1-3}H_xO]^+$ [24,53] where the oxygen comes from residual water outgassing from the reactor walls. Mandich and Reents[53] have demonstrated that a 5 % water-in-silane mixture leads to indefinite polymerisation via positive ions. However, we do not expect to have such a high water content when the hot reactor is freshly-covered with a-Si:H, and indeed the oxide contribution is only 0.8 % of the total positive ion spectrum which is in any case limited to 150 amu here. This is further evidence that there is probably no unique pathway for polymerisation in silane-containing gases and plasmas. Oxides are completely absent in the negative ion mass spectrum in Figure 10.

The raw data in Figure 10 represent the ion fluxes, not the ion plasma densities, and are uncorrected for charge- and mass-dependent effects which could strongly modify the true relative ion abundances. These effects can be considered as two processes, ion extraction from the plasma followed by transmission and detection in the mass spectrometer :

i) For extraction from the plasma, the drift velocity varies as the inverse square root of the ion mass[27] (see Fig.9) which discriminates against heavy ion intensities[31] of both charge types. The negative ions also arrive at the orifice with less energy than positive ions as shown in Fig. 4, although the solid angle of acceptance into the orifice is consequently expected to be larger for negative ions.[59] Collisional break-up of large, weakly-bonded cluster ions of both charge signs could occur on passing through the orifice,[56] although the relative abundances were insensitive to different extraction voltages.

ii) The transmission efficiency of the mass spectrometer is expected to be charge-independent since the electrode voltages used for negative ions were simply the reverse of the voltages used for positive ions. Quadrupole mass filter transmission and channeltron sensitivity

both decrease with mass for both charge signs but the calibration of the mass spectrometer is unknown for high masses and consequently the data have not been corrected for this effect.

The combination of these two processes means that the relative density of heavy ions of both types will be higher in the plasma than implied by the relative abundances in Fig. 10. The density of negative relative to positive ions is difficult to quantify because of the different plasma conditions (afterglow and power on period respectively) during extraction of each type from the plasma.[50] Nevertheless, it is unlikely that any charge-dependent correction factor would increase faster than exponentially with mass (see Fig. 12 below) and so we can conclude from Fig. 10 that the negative ions attain much higher masses than the positive ions.

Figure 11 shows that significant amounts of di- and tri-silane exist for our plasma conditions, but only trace quantities of tetrasilane radicals are detected with no higher-mass neutrals present in the spectrum. This measurement is consistent with the observation, in Fig. 7, that attachment peaks are essentially absent for masses higher than trisilane and demonstrates that no heavier neutrals are available in the discharge volume for electron attachment once the plasma is extinguished.

The relative abundances of the neutrals and the positive and negative ions for a 1 kHz modulation frequency are shown in Figure 12 taken from Figs. 10 and 11. The first two negative ion groups vary strongly with modulation frequency and are omitted from the figure. The intensity mass-dependence is approximately exponential with fall-off ratios for consecutive masses of 0.65 for negative ions, 0.24 for positive ions, and 0.05 for the neutrals. Haller[22] showed that the positive ion ratio varies between 0.2 and 0.33 over a wide range of rf silane plasma conditions and that the decrease in neutral concentrations is much more rapid, in good agreement with our results. It was deduced that the heavy positive ions do not arise from electron impact ionisation of correspondingly-heavy neutrals because a rapid increase in ionisation efficiency with size is highly unlikely.[22] The implication was that the positive ions are formed in a chain reaction by silane addition as suggested also by Weakliem[24] and others. Equivalently, it would appear from our results in Fig. 12 that the negative ions are also formed in a chain reaction, and not by electron attachment to heavy neutrals, because such a rapid increase in attachment efficiency with mass is improbable.

Figure 13 shows how the time-averaged negative and positive ion signals vary with modulation frequency. The negative ion signals are expressed in counts per modulation cycle whereas the positive ion intensity is given in counts per second; this reflects the different mechanisms by which the ions escape from the plasma : the observed positive ion intensity is due to a continual flux during the plasma period, whereas the observed negative ion signal is due to a pulse when the accumulated negative ion density escapes in the afterglow.

A striking feature of Fig. 13 is that the positive ion intensity and spectrum are almost independent of modulation frequency in contrast to the strong variation in negative ion intensities. This is probably because the modulation duty cycle is constant (at 50 %) so that the positive ion flux duration is independent of the modulation frequency. Similar observations have been made in other plasmas.[30,50]

All negative ion intensities fall to zero for modulation frequencies higher than 15 kHz. The afterglow period at this frequency is 33 μs which corresponds to the delay obtained by extrapolation of the negative ion delay time as explained in Section IIIB for Fig. 6. The sheath electric field, above 15 kHz modulation frequency, does not have time to reverse and so the negative ions remain trapped in the plasma volume and continue to accumulate during successive plasma cycles and polymerise indefinitely, leading to powder particles as observed in Ref 33.

IV. DISCUSSION & PLASMA POLYMERISATION SCHEME

A. Formation of polysilicon hydride anions

The experimental results suggest that a polymerisation pathway proceeds via negative ion clustering. The negative ions are not simply by-products formed by electron attachment to a neutral species pathway. To recapitulate, three reasons why the high-mass negative ions are not formed by attachment to heavy neutrals are :

i) no neutrals with masses as high as negative ions are detected in the mass spectra (Figs. 10 and 11),

ii) negative ions and neutrals have very different abundance ratios which cannot be reasonably explained by supposing attachment probabilities which are orders of magnitude larger for higher masses (Fig. 12), and

iii) no attachment peaks exist in the time-resolved measurements for negative ions heavier than trisilicon hydride anions (Fig. 7).

One possible polymerisation pathway which propagates via negative ions is by silane addition,[27] analogous to the condensation reactions proposed for positive ions.[20,22,24] Since it is necessary to explain cluster growth, only non-dissociative reactions will be considered for the following reactions :

$$\text{silane addition :} \quad Si_nH_x^- + SiH_4 \rightarrow (Si_{n+1}H_{x'}^-)^* + (H, H_2 \text{ products}). \qquad (1)$$

In this ion-molecule reaction, the excited negative ion can relax by redistribution of its excess energy amongst internal, ro-vibrational modes; this is consequently more efficient for large negative ions.[62] Alternatively, the negative ion can lose its excess energy by a stabilisation collision with a third body which must occur within its auto-detachment lifetime if the parent ion is to survive[63]:

$$\text{stabilisation collision :} \quad (Si_nH_x^-)^* + M \rightarrow Si_nH_x^- + M. \qquad (2)$$

The stable negative ion in this case results from a second order reaction. If the excess energy is not dissipated sufficiently rapidly, the parent ion will be destroyed by auto-detachment :

$$\text{auto-detachment :} \quad (Si_nH_x^-)^* \rightarrow Si_nH_x + e^-. \qquad (3)$$

Ion-ion recombination is the second possible pathway for polymerisation [64,65]:

$$\text{ion-ion recombination :} \quad Si_nH_x^- + Si_pH_q^+ \rightarrow Si_{n'}H_{x'} + (Si, H, H_2 \text{ products}) \qquad (4)$$

The rate coefficients for recombination of small or large clusters have been shown to be similar.[66] Here, the increase from n to n' silicon atoms could be larger than one because of the

existence of positive ions up to pentasiliconium. Negative ion production by electron impact ion pair creation is energetically unlikely for the low electron temperatures commonly found in rf silane plasmas.

Reactions (3) and (4) both result in a neutral cluster and since heavy neutrals are not observed, it must be supposed that they are re-attached :

$$\text{attachment :} \qquad Si_nH_x + e^- \rightarrow (Si_nH_x^-)^* \rightarrow Si_nH_x^-. \qquad (5)$$

Low-energy electron attachment in which the parent negative ion survives against dissociation or auto-detachment has been shown to be the dominant channel in the case of large clusters.[55] Therefore the ion-molecule and ion-ion reactions both eventually lead to stable, higher-mass negative ions.

Large, hydrogenated silicon clusters are electronegative (electron affinity > 1.4 eV)[64] since they form stable negative ions. Their lifetime is greater than 100 μs because they survive the transit through the mass spectrometer. The discussion above shows that other conditions for the existence of these negative ionic clusters are that secondary, polymerising reactions occur with silane molecules or positive ions; that excess energy can be rapidly dissipated by stabilising collisions; and that electrons are available for attachment. A further important condition is that negative ions should have sufficient time to undergo many collisions in the plasma. All of these conditions are satisfied in the silane plasma deposition experiment at 0.1 mbar since high densities of silane molecules, positive ions and electrons are available, and the negative ions are trapped almost indefinitely in the plasma by the sheath potentials.

In contrast, previous studies of clustering in silane plasmas have used very low silane pressures and environments which are different from plasma deposition conditions. For example, Fourier Transform Mass Spectrometer (FTMS) experiments[19,52,67] operating at pressures of 1-10 x 10^{-7} mbar with reaction times of 0.01 - 10 s concluded that negative ions had no reactions with silane on the experimental timescales investigated. However, the ion-molecule reaction rate in (1) above, assuming auto-stabilisation of the negative ion, is proportional to the silane pressure. Therefore, a 1 s FTMS experiment at 5 x 10^{-7} mbar is

equivalent to only 5 μs at the pressures used for the experiments in this paper. Conversely, a single power modulation cycle at 1 kHz corresponds to 200 seconds of confinement in a FTMS cell. Reactions requiring third body stabilisation impose far more severe time constraints on low pressure experiments. In a plasma environment, ion-ion reactions, reactive radicals and species in excited rovibrational and electronic states will strongly affect reaction cross-sections, whereas FTMS experiments are generally relevant only to reactions with ground state molecules.[67] Crossed electron beam-molecular beam collision experiments using silane[54] are designed to avoid secondary processes and multiple collisions, and so it is not surprising that very large negative ionic clusters in silane have not been previously observed.

B. Polymerisation scheme for negative ions

The qualitative behaviour of negative ion polymerisation in modulated silane plasmas can be described by a phenomenological model, although a full description with a self-consistent treatment of electrons, positive and negative ions and electric fields is beyond the scope of this paper. The observed negative ion flux is convoluted by the action of the sheath in modulated plasmas,[50] and so a model is needed to extrapolate back from the observed flux to the negative ion density in the plasma bulk. Quantitative predictions are not possible here because the cross-sections for the heavy negative ionic cluster reactions are unknown and, in any case, the measurements were not made in the electrode but in the plasma edge. The aim is first of all to discover which species is responsible for powder formation since this is not yet clear.[19]

Previous plasma simulations have not included large negative ionic clusters because their existence was unknown. Instead, the reason for including negative ions was because a large fraction of negative mono- or di-silicon hydride anions created by dissociative attachment would affect the plasma properties by changing the electron/positive ion ratio.[20] The predictions of a fluid equation model developed by Overzet *et al* [31] for the negative ion flux during the afterglow of a modulated plasma enabled us to interpret the experimental results given in Section IIIB. However, polymerisation was not explicitly included in that model.

In the following, the term $S_n(t)$ designates the time-varying density of all the polysilicon hydride anions containing n silicon atoms (thus representing the low mass resolution measurements) :

$$\text{polysilicon hydride anion density :} \qquad S_n(t) = \sum_x Si_nH_x^-. \tag{6}$$

The conservation equation for the monosilicon hydride anion density is :

$$\text{monomer :} \qquad dS_1(t) / dt = f(t) - K_1S_1(t) - g_1(t), \tag{7}$$

where f(t) is the monomer source term due to electron attachment on silane, K_1 is the reaction rate for silane addition, and $g_1(t)$ is the monomer loss rate due to detachment and modulation losses. For simplification of the model, we will arbitrarily assume that polymerisation proceeds by ion-molecule reactions (Eq. (1)) and neglect ion-ion recombination (Eq. (4)) in what follows. The reaction rate K_1 (units s^{-1}) includes all the ion-molecule reactions which result in a disilicon hydride anion by silane addition to a monosilicon hydride anion. For the remaining equations we ignore formation of higher-mass negative ions S_n ($n > 1$) by any process other than by polymerisation from the preceding S_{n-1} ion, to obtain :

$$\text{polysilicon hydride anions :} \qquad dS_n(t) / dt = K_{n-1}S_{n-1}(t) - K_nS_n(t) - g_n(t). \tag{8}$$

Equation (8) is the general conservation condition for these ions which includes polymerisation terms and where there is no attachment due to the absence of polysilane neutrals. The function $g_n(t)$ represents modulation-induced loss rates due to the sheath collapse which are considered to be large compared to the weak transverse diffusion losses out from between the electrodes. Any detachment losses are ignored for the heavy ions because it is assumed that re-attachment would occur before the neutral product could leave the discharge volume. Time-averaging over a power modulation cycle in steady-state conditions and adding the first N equations gives :

$$\text{mean polysilicon hydride anion density :} \qquad \overline{S_N} = (\bar{f} - \sum_1^N \overline{g_n}) / K_N \tag{9}$$

where it is assumed that there is no break in the polymerisation sequence since all K_n are taken to be non-zero. Equation (9) shows that the time-averaged plasma density of the polymerised negative ion S_N is determined by the monosilicon hydride anion production rate, the polymerisation reaction rate K_N for the ion itself, and the total of the modulation-induced losses of all the preceding negative ions. This emphasises the importance of power modulation for controlling the density of negative, highly-polymerised species in the plasma.

In order to investigate the effect of modulation frequency on the ion densities, the values of the monosilicon hydride anion source term f(t) and all the loss terms $g_n(t)$ and reaction rates K_n must be estimated :

The initiating step is the formation of monosilicon hydride anions by dissociative attachment to silane :

$$\text{initiating step :} \qquad SiH_4 + e^- \rightarrow SiH_x^- + ((4-x)\ H \text{ products}). \tag{10}$$

The lowest appearance potential (6.5 eV) and the largest cross-section (19×10^{-19} cm^2)[52] is for SiH_3^- and this is in fact the dominant monosilicon hydride anion observed in these plasmas.[33] The source term is therefore:

$$\text{source term :} \qquad f(t) = n_e(t)\ [SiH_4]\ \langle \sigma_{att} v_e \rangle, \tag{11}$$

where σ_{att} is the total cross-section for all dissociative attachment reactions with silane. The electron density and distribution function will vary during the plasma period, especially during the initial transient phase,[10] but f(t) will be assumed here to be constant during the plasma for all modulation frequencies. The most energetic electrons disappear within micro-seconds of the end of the plasma period, and since the appearance potentials for attachment to silane are 6.5 eV or larger,[52] we set f(t) = 0 during the afterglow. The magnitude of f(t) in the model is only a scale factor for the negative ion densities and does not influence their temporal behavior.

The loss rate $g_n(t)$ is due to the negative ion diffusion which arises after the delay interval during the afterglow. Figures 7 and 5 show that the ion densities decay approximately exponentially, and so we rewrite equation (8) as :

$$\text{polysilicon hydride anions :} \quad dS_n(t)/dt = K_{n-1}S_{n-1}(t) - (K_n + D_n)S_n(t), \tag{12}$$

where $D_n \neq 0$ only in the afterglow after the corresponding delay interval for the n^{th} polysilicon anion. The delays were estimated for n = 1 to 6 and for all modulation frequencies by extrapolation from the experimental data in Figures 9 and 6. Note that ion-molecule polymerisation continues throughout the cycle, independently of the modulation-induced losses. We assume the diffusion constant D_n to be inversely proportional to the square root of the anion mass ($D_n = D / \sqrt{n}$) and so the loss rate terms become :

$$\text{loss rate approximation :} \quad g_n(t) = S_n(t)\, D / \sqrt{n} \tag{13}$$

where D is an empirical diffusion constant.

The negative ion densities for a given modulation frequency were then determined by iterating equations (7) and (12) until the time-variation of each ion density was the same in successive cycles, giving steady-state time-averaged densities. Values for D and K_n (see below for discussion) were self-consistently chosen so that the calculated losses in Figures 14(b) and 15(b) reproduced the experimental data in Figures 7 and 13 as accurately as possible for mono- to hexa-silicon hydride anions, given the limitations imposed by the assumptions made in the model. Note that attachment effects which are responsible for the initial peaks in Fig. 7 are neglected in this model because the increment in the negative ion time-averaged intensities due to attachment is small compared to their intensity variations with modulation frequency shown in Figs. 13 and 15(b). The agreement between model and experiment is qualitatively reasonable and so the model can be used to estimate the temporal behavior of the negative ion densities within the plasma as shown in Figures 14(a) and 15(a).

Figure 14(a) shows the calculated time-dependence of the first six negative ion groups for a 1 kHz modulation frequency. The density of the higher polysilicon hydride ions S_n (n > 2) rises during the plasma period and continues to rise during the first part of the afterglow because polymerisation of the preceding ion S_{n-1} with the silane gas proceeds independently of the plasma period. The negative ion densities begin to fall after the respective delay interval for

each ion due to diffusion losses to the electrodes; these calculated losses are shown in Fig. 14(b).

Figure 15(a) shows the calculated modulation frequency-dependence of the negative ion densities in the plasma. In a continuous plasma, the density of each ion would be $S_n = f / K_n$ (from equation (9) with all $g_n = 0$). For very low modulation frequencies, the ion densities have time to reach these equilibrium values during the plasma which then fall to zero during the 'off' period. The time-averaged densities are therefore $S_n \approx f / 2K_n$ for a 50 % duty cycle in the limit of low modulation frequency - this is the situation for frequencies below 0.1 kHz as can be seen in Figure 15(a), and the observed losses in Figure 15(b) correspond to the negative ions which escape during the 'off' periods. At frequencies above 15 kHz, however, no negative ions escape because the afterglow period is shorter than the delay interval and there are no observed losses for this high frequency range. The negative ions attain a density where the monosilicon hydride anion production compensates for polymerisation losses for each ion type, and this again corresponds to time-averaged densities where $S_n = f / 2K_n$ for a 50 % duty cycle at high modulation frequency. The negative ion densities in the limits of high and low modulation frequency are therefore the same and are half of the continuous plasma values.

In the intermediate frequency range around 1 kHz, the densities decrease strongly for the higher masses, and the hexasilicon hydride anion density is reduced by almost an order of magnitude. Physically, this is because the plasma period is too short for the polymerisation chain to propagate from mono-silicon to highly-polymerised species before almost all of the low mass species are again lost in the subsequent 'off' period. Equilibrium between the diminished supply from preceding negative ions and the polymerisation of the polysilicon hydride anion itself results in a strongly-reduced density of the highly-polymerised anions. *This is a key result which explains why powder reduction can occur at kHz square-wave modulation frequencies.* This picture is similar to that in our previous paper[33] and will be discussed further in the following sub-section.

The forms of the curves in Figs.14(b) and 15(b) are sensitive to the choice of the polymerisation reaction rates K_n. In order to obtain a satisfactory agreement with experiment, it was necessary to put $K_1 = 10^4$ s^{-1}, followed by $K_2 = 2.5 \times 10^3$ s^{-1} with subsequent K_n values

increasing gradually from 2.5 x 10^3 s^{-1} to 4 x 10^3 s^{-1} for hexasilicon hydride anions. For the pure silane plasma at 0.1 mbar, assuming anion reactions with silane molecules, this is equivalent to rate constants of 4 x 10^{-12} cm^3s^{-1} for all the combined mono-silicon group reactions and from 10^{-12} to 1.6 x 10^{-12} cm^3s^{-1} for the higher polysilicon hydride anion-molecule reactions in equation (8). These estimated reaction rates are below the detection limit of 10^{-11} cm^3s^{-1} for the FTMS experiments of Haaland[52] and are 20 to 500 times slower than typical low-mass positive ion-molecule exothermic reactions in silane.[67-69] The value of the empirical diffusion constant D (1.1 x 10^4 s^{-1} for these results) was less critical for a match with experimental data.

The rapid reaction rate of the monosilicon hydride anions relative to the high-mass anions would explain why their density is lower than the heavier negative ion densities (except for modulation frequencies near 1 kHz); a low negative monomer density has also been reported for boron trichloride rf plasmas.[51] Resonance effects due to the like masses of monosilicon hydride anions and silane molecules could be responsible for this enhancement by a factor of four for K_1 with respect to K_2. The efficiency of excess energy re-distribution in larger ionic molecules could possibly explain the gradually-increasing reaction rates for the higher-mass negative ions.

The polymerisation model above presupposed anion-molecule chain reactions as in equation 1. Anion-radical reactions might be responsible for the polymerisation chain if anions are unreactive towards silane molecules,[64] in which case the estimated cross-sections would be larger in inverse proportion to the fractional radical density in the silane gas. Ion-ion recombination followed by electron attachment[52,65] (see Eqs. (4) and (5)) also results in polymerised negative ions and should therefore be considered. However, since the degree of ionisation of this type of plasma is expected to be about 10^{-6}, the ion-ion reaction would have to be at least 10^6 times faster than the ion-molecule rate for the ion-ion pathway to be important. The rate constant for ion-ion recombination[62] is approximately 10^{-7} cm^3s^{-1} which is therefore too small, when multiplied by the ionisation degree, to account for the estimated polymerisation rate constants of 10^{-12} cm^3s^{-1}. When attachment is included, the overall rate is still further reduced. Nevertheless, since the polysilicon hydride anion-molecule rate constants are

unknown, it is not possible here to determine the relative importance of anion-molecule and ion-ion reactions.

C. Powder formation in modulated plasmas

The negative ion condensation model for the primary growth of plasma particulates is too simplistic to cover the whole range of powder development up to visible particles, and an interdisciplinary approach involving the physics of plasmas, clusters and nucleation dynamics is called for. This paper is restricted to a study of the initial phase of particle growth which is nevertheless crucial to the understanding of powder production.[28]

Boufendi *et al*,[70] working in argon-diluted silane plasmas, have shown that an unidentified, initial clustering step produces nuclei of less than 5 nm in about 0.5 s. This size corresponds to about 10^4 silicon atoms. The subsequent increase in particle diameter of 10 nm s^{-1},[70] which is more than an order of magnitude faster than the polymerisation rate which forms the initial nucleus, could be by agglomeration of the initial clusters[70,71] or by accretion of neutral radicals or positive ions across the particle sheath which forms when the particle is large enough.[28,60,61]

Taking the polymerisation rate constant for clusters to be 1.6×10^{-12} cm^3s^{-1} from Section IVB, and since the number of silicon atoms increases linearly with time in our model, we estimate approximately 2.5 s for the formation time of a nucleus containing 10^4 silicon atoms for our plasma parameters. Powder particles grow large enough to be visible after 30 s of continuous rf power in our plasma conditions.[72]

On the basis of these observations, the dependence on modulation frequency for powder formation in modulated plasmas would be as follows[12]:

At modulation frequencies much less than 1 kHz, large clusters or even particles form within a single plasma period and some may become too large to be ejected in the subsequent 'off' period; these particles would then continue to grow during successive cycles and eventually become visible.[8,12] Andújar *et al* [13] have shown that poor quality amorphous silicon films are produced when large clusters or particles fall onto the film surface during deposition under these conditions.

At modulation frequencies closer to but still less than 1 kHz, clusters do not grow too large in one plasma cycle to be ejected in the 'off' period and the plasma appears powder free.[4,11] Plasma parameters determine the polymerisation rate and consequently the modulation frequency below which powder becomes visible as described above.

At approximately 1 kHz modulation frequency, the plasma period is too short for polymerisation to propagate, as explained in section IVB, and powder production is suppressed.[4,10,11,29] The best film quality is obtained at this modulation frequency.[13] The basic polymerisation model described above shows that the suppression of highly-polymerised species at this frequency is even more efficient for lower duty cycles (such as 25 % or lower), since then the reservoir of disilicon hydride anions can diffuse away more completely in the longer afterglow period. Other forms of power modulation, for example, by varying the rf power during each cycle or over many cycles, could possibly be used to advantage.

Above 1 kHz modulation frequency , the negative ions are trapped by the sheath potentials which do not have time to reverse and polymerisation continues in successive modulation cycles, ultimately forming particles in the plasma. These particles acquire a multiple electronic charge in the plasma and therefore remain trapped. Visible powder begins to accumulate simultaneously with the disappearance of the negative ion observed loss flux, as has been demonstrated by experiment .[33]

Substrate heating above ambient temperature reduces powder formation[17,72] and increases the flux of elementary negative ions from the plasma[32]; it appears that clustering reactions are inhibited by heating of the gas.[7] Since dissociative attachment cross-sections increase[63] and ion-ion recombination rates decrease[62] with increasing gas temperature, these experimental observations are consistent with the hypothesis that gas heating inhibits the clustering of negative ions.[64] Various methods, separately or combined with power modulation, could be envisaged to eliminate particle contamination during silane plasma processing by inhibiting the polymerisation sequence propagated via negative ions.

V. CONCLUSIONS

The time-resolved fluxes of negative ionic clusters from a power-modulated rf silane plasma have been measured by mass spectrometry. These polysilicon hydride anions diffuse from the plasma with low energy (approximately 0.5 eV) during the afterglow when the electron density has decayed and the sheath electric fields reverse. Measurements of these fluxes for different anion masses and modulation frequencies demonstrate that the plasma composition is influenced by the modulation frequency.

The negative species attain much higher masses than the positive or neutral species and it is proposed that a polymerisation pathway propagates via the negative ions. A simple polymerisation scheme is described which qualitatively reproduces the experimental results and shows that the densities of high mass negative ions are strongly reduced by modulation frequencies near 1 kHz. Each plasma period is then too short for the polymerisation chain to propagate to high masses before the elementary anions are lost in each subsequent afterglow period - this explains why modulation of the rf power can reduce particle contamination. The presence of highly-polymerised negative ions fundamentally changes the conventional view of rf silane plasmas.

There is no unique clustering reaction for producing particles in processes using reactive gases or plasmas, and the mechanisms of initiation, nucleation and particle growth are also likely to be different for any given process. The conclusion of this paper is that, for the case of silane rf plasmas used for amorphous silicon deposition, the initiation steps proceed by negative ion polymerisation.

ACKNOWLEDGEMENTS

We are indebted to Dr. J. Perrin for valuable suggestions and his advice concerning the literature on negative ion research. We also thank Peter Hatton and colleagues of Hiden Analytical Limited. This work was funded by the Swiss Department of Energy Grant no. EF-REN(91)31 and by Swiss Federal Research Grant no. BBW.EG(91)3 (for BRITE/EURAM contract BE-4529-90).

REFERENCES

[1]G. S. Selwyn, J. Singh and R. S. Bennett, J. Vac. Sci. Technol. A **7**, 2758 (1989).

[2]G. S. Selwyn, J. S. McKillop, K. L. Haller and J. J. Wu, J. Vac. Sci. Technol. A **8**, 1726 (1990).

[3]G. S. Selwyn, J. E. Heidenreich and K. L. Haller, J. Vac. Sci. Technol. A **9**, 2817 (1991).

[4]Y. Watanabe, M. Shiratani, Y. Kubo, I. Ogawa and S. Ogi, Appl. Phys. Lett. **53**, 1263 (1988).

[5]W. J. Yoo and Ch. Steinbrüchel, J. Vac. Sci. Technol. A **10**, 1041 (1992).

[6]K. G. Spears, T. J. Robinson and R. M. Roth, IEEE Trans. Plasma Sci. **14**, 179 (1986); and K. G. Spears, R. P. Kampf, and T. J. Robinson, J. Phys. Chem. **92**, 5297 (1988).

[7]A. Bouchoule, A. Plain, L. Boufendi, J. Ph. Blondeau and C. Laure, J. Appl. Phys. **70**, 1991 (1991).

[8]A. A. Howling, Ch. Hollenstein and P.-J. Paris, Appl. Phys. Lett. **59**, 1409 (1991).

[9]Y. Watanabe, M. Shiratani and M. Yamashita, Appl. Phys. Lett. **61**, 1510 (1992).

[10]J. T. Verdeyen, J. Beberman, and L. Overzet, J. Vac. Sci. Technol. A **8**, 1851 (1990).

[11]Y. Watanabe, M. Shiratani and H. Makino, Appl. Phys. Lett. **57**, 1616 (1990).

[12]A. Lloret, E. Bertran, J. L. Andújar, A. Canillas, and J. L. Morenza, J. Appl. Phys. **69**, 632 (1991).

[13]J. L. Andújar, E. Bertran, A. Canillas, J. Campmany, J. Serra, C. Roch and A. Lloret, J. Appl. Phys. **71**, 1546 (1992).

[14]W. Siefert, Thin Solid Films **120**, 267 (1984).

[15]R. C. Ross and J. Jaklik, Jr., J. Appl. Phys. **55**, 3785 (1984).

[16]N. Morosoff, *Plasma Deposition, Treatment, and Etching of Polymers* (Academic Press 1990) ed. R. d'Agostino.

[17]A. M. Wróbel and M. R. Wertheimer, ibid.

[18]H. Yasuda, *Plasma Polymerisation* (Academic Press 1985)

[19]M. L. Mandich, W. D. Reents, and K. D. Kolenbrander, Pure & Appl. Chem. **62**, 1653 (1990).

[20]M. J. Kushner, J. Appl. Phys. **63**, 2532 (1988).

[21]S. Veprek, K. Schopper, O. Ambacher, W. Rieger and M. G. J. Veprek-Heijman, submitted to J. Electrochem. Soc.

[22]I. Haller, Appl. Phys. Lett. **37**, 282 (1980).

[23]T. P. Martin and H. Schaber, J. Chem. Phys. **83**, 855 (1985).

[24]H. A. Weakliem, R. D. Estes, and P. A. Longeway, J. Vac. Sci. Technol. A **5**, 29 (1987).

[25]H. M. Anderson, R. Jairath, and J. L. Mock, J. Appl. Phys. **67**, 3999 (1990).

[26]H. Chatham and A. Gallagher, J. Appl. Phys. **58**, 159 (1985).

[27]J. Perrin, A. Lloret, G. de Rosny, and J. P. M. Schmitt, Int. J. Mass Spectrom. Ion Processes **57**, 249 (1984).

[28]A. Garscadden, NATO ASI Series B: Physics Vol. 220. *Nonequilibrium Processes in Partially Ionised Gases* , edited by M. Capitelli and J. N. Bardsley, (Plenum, New York, 1990), p. 541; and
A. Garscadden, Proc. XXth Int. Conf. in Ionised Gases (Pisa), Invited Paper (1991) p147.

[29]R. W. Boswell and D. Vender, IEEE Trans. on Pl. Sci. **19**, 141 (1991).

[30]Y. Lin and L. J. Overzet, Appl. Phys. Lett. **62**, 675 (1993).

[31]L. J. Overzet, Y. Lin and L. Luo, J. Appl. Phys. **72**, 5579 (1992) and L. J. Overzet, to appear in J. Vac. Sci. Technol. A.

[32]A. A. Howling, L. Sansonnens, J.-L. Dorier, and Ch. Hollenstein, J. Phys. D: Appl. Phys. **26**, 1003 (1993).

[33]A. A. Howling, J.-L. Dorier, and Ch. Hollenstein, Appl. Phys. Lett. **62**, 1341 (1993).

[34]S.-K. Park and D. J. Economou, J. Appl. Phys. **68**, 3904 (1990).

[35]J. Kramer, J. Appl. Phys. **60**, 3072 (1986).

[36]M. Haverlag, A. Kono, D. Passchier, G. M. W. Kroesen, W. J. Goedheer and F. J. de Hoog, J. Appl. Phys. **70**, 3472 (1991).

[37]A. Kono, M. Haverlag, G. M. W. Kroesen and F. J. de Hoog, J. Appl. Phys. **70**, 2939 (1991).

[38]C. B. Fleddermann, J. H. Beberman and J. T. Verdeyen, J. Appl. Phys. **58**, 1344 (1985).

[39]R. A. Gottscho and C. E. Gaebe, IEEE Trans. on Pl. Sci. **PS-14**, 92 (1986).

[40]R. A. Gottscho, Phys. Rev. A **36**, 2233 (1987).

[41]R. Deutsch and E. Räuchle, Phys. Rev A **46**, 3442 (1992).

[42]J. P. Boeuf, Phys. Rev. A **36**, 2782 (1987).

[43]C. Böhm and J. Perrin, J. Phys. D: Appl. Phys. **24**, 865 (1991).

[44]J. P. Boeuf, Ph. Belenguer and J. Wang, Mater. Res. Soc. Symp. Proc. **165**, 17 (1990).

[45]F. Tochikubo, A. Suzuki, S. Kakuta, Y. Terazono and T. Makabe, J. Appl. Phys. **68**, 5532 (1990).

[46]M. Shiratani, T. Fukuzawa, K. Eto and Y. Watanabe, Jpn. J. Appl. Phys. **31**, L1791 (1992).

[47]L. J. Overzet and J. T. Verdeyen, Appl. Phys. Lett. **48**, 695 (1986).

[48]J. L. Jauberteau, G. J. Meeusen, M. Haverlag, G. M. W. Kroesen and F. J. de Hoog, Appl. Phys. Lett. **55**, 2597 (1989).

[49]H. Amemiya, J. Phys. D: Appl. Phys. **23**, 999 (1990).

[50]L. J. Overzet, J. H. Beberman and J. T. Verdeyen, J. Appl. Phys. **66**, 1622 (1989).

[51]L. J. Overzet and L. Luo, Appl. Phys. Lett. **59**, 161 (1991).

[52]P. Haaland, J. Chem. Phys. **93**, 4066 (1990).

[53]M. L. Mandich and W. D. Reents, J. Chem. Phys. **96**, 4233 (1992).

[54]S. K. Srivastava, E. Krishnakumar and A. C. de A. e Souza, Int. J. Mass Spectrom. Ion Processes. **107**, 83 (1991).

[55]I. Sauers, L. G. Christophorou, and J. G. Carter, J. Chem. Phys. **71**, 3016 (1979).

[56]D. Smith and I. C. Plumb, J. Phys. D: Appl. Phys. **6**, 1431 (1973).

[57]A. A. Howling, J.-L. Dorier, Ch. Hollenstein, F. Finger and U. Kroll, J. Vac. Sci. Technol. A **10**, 1080 (1992).

[58]K. Köhler, J. W. Coburn, D. E. Horne and E. Kay, J. Appl. Phys. **57**, 59 (1985).

[59]Hiden Analytical Limited, Gemini Business Park, Warrington WA5 5TN, UK

[60]M. J. McCaughey and M. J. Kushner, J. Appl. Phys. **69**, 6952 (1991).

[61]J. E. Daugherty, R. K. Porteous, M. D. Kilgore, and D. B. Graves, J. Appl. Phys. **72**, 3934 (1992).

[62]A. P. Hickman, J. Chem. Phys. **70**, 4872 (1979).

[63]L. G. Christophorou, Environmental Health Perspectives **36**, 3 (1980).

[64]J. Perrin, private communication.

[65]J. Perrin and J. Schmitt, Proc. 11th Eur. Photovoltaic Solar Energy Conf., Montreux (1992) p80.

[66]D. Smith, M. J. Church and T. M. Miller, J. Chem. Phys. **68**, 1224 (1978).

[67]M. L. Mandich and W. D. Reents, J. Chem. Phys. **90**, 3121 (1989).

[68]W. D. Reents and M. L. Mandich, J. Chem. Phys. **96**, 4429 (1992).

[69]M. L. Mandich and W. D. Reents, J. Chem. Phys. **95**, 7360 (1991).

[70]L. Boufendi, A. Plain, J. Ph. Blondeau, A. Bouchoule, C. Laure, and M. Toogood, Appl. Phys. Lett. **60**, 169 (1992).

[71]I. Goldhirsch and G. Zanetti, Phys. Rev. Lett. **70**, 1619 (1993).

[72]J.-L. Dorier, Ch. Hollenstein, A. A. Howling and U. Kroll, J. Vac. Sci. Technol. A **10**, 1048 (1992).

FIGURE CAPTIONS

FIG. 1 Schematic drawing of the reactor and mass spectrometer with a block diagram of the rf power modulation and time-resolved acquisition system.

FIG. 2 Estimation of the ion transit times in the mass spectrometer. The data points were estimated from experiments performed for ion masses up to 178 amu. The straight line is calculated from the known ion energies and trajectories within the mass spectrometer. Negative ions = •; positive ions = o.

FIG. 3 Time-resolved normalised intensities of $Si_2H_5^+$ ions (o) and $Si_2H_5^-$ ions (•), each compared with the SiH* emission (heavy line) for a 2 kHz-modulated plasma. The time origin is referenced to the start of the plasma period.

FIG. 4 Time-averaged energy spectra of $Si_2H_5^+$ and $Si_2H_5^-$ ions for the plasma conditions in Fig. 3. Each data point was acquired with a dwell time of 300 ms, that is, time-integrated over 600 power modulation cycles.

FIG. 5 $Si_2H_5^-$ intensities expressed as the number of counts in 10'000 gates of time width 5 μs, for power modulation frequencies of 0.5, 1, 2 and 5 kHz. One power modulation cycle is shown for each, with time referenced to the beginning of the afterglow period. The plasma duration is represented by the heavy line.

FIG. 6 Dependence on modulation frequency of the $Si_2H_5^-$ signal onset delay time taken from Fig. 5. The afterglow period (heavy line) is half of the inverse modulation frequency.

FIG. 7 Time-resolved fluxes for mono- to hexa-silicon hydride negative molecular ion groups for a 1 kHz power modulation frequency. Time is referenced to the beginning of the afterglow period, the plasma duration is represented by the heavy line.

FIG. 8 Normalised intensities of the positive polysiliconium ions for plasma parameters identical to those in Fig. 7.

FIG. 9 Mass-dependence of the positive ion decay time constants and onset delay times for negative ion signals, taken from Figs. 8 and 7 respectively.

FIG. 10 Mass spectra of negative and positive molecular ion groups for a 1 kHz power modulation frequency, time-averaged over 300 modulation cycles. This raw data, acquired with

low mass resolution, is uncorrected for any mass-dependent fall-off in sensitivity. The vertical broken lines at intervals of 28 amu mark the masses of bare silicon clusters.

FIG. 11 Ion currents for polysilane molecules ionised by 20 eV electrons in the mass spectrometer. Plasma parameters are the same as for Fig. 10. The spectrum has been corrected for the background signal due to filament outgassing in the spectrometer. Only monosilane was detected with the rf power off.

FIG. 12 Relative ion currents measured for negative and positive ions and for ions formed from neutral radicals in the mass spectrometer ioniser by 20 eV electrons. Modulation frequency 1 kHz. The straight lines are exponential fits to the data which are normalised to unity for the mono-silicon groups.

FIG. 13 Variation of negative and positive ion signals as a function of modulation frequency. The negative ion intensities have been divided by the modulation frequency to give the total loss counts per modulation cycle. The signal for each ion is the integral over the mass profile of each ion group (as shown in the time-averaged mass spectrum in Fig. 10 for 1 kHz) for different modulation frequencies.

FIG. 14 Calculated time-dependences, during one power modulation cycle at 1 kHz, for the first six polysilicon hydride anions : (a) estimated anion densities in the plasma; (b) the corresponding anion loss flux estimates. The plasma duration is represented by the heavy line.

FIG. 15 Calculated modulation frequency-dependences for the first six polysilicon hydride anions : (a) estimated time-averaged anion densities in the plasma; (b) the corresponding time-averaged anion loss flux estimates.

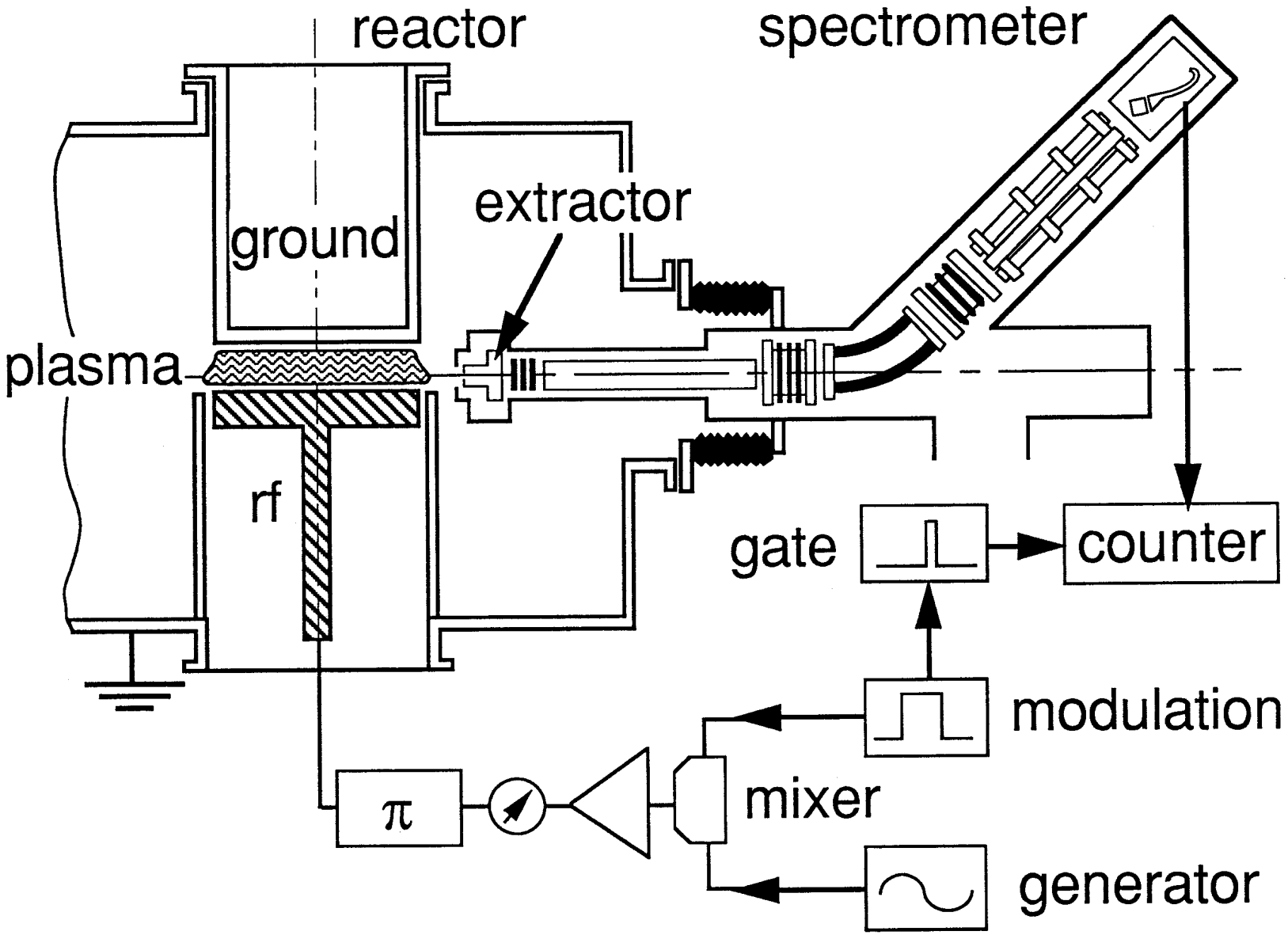

Fig 1 of 15
A A Howling
"Time-resolved..."

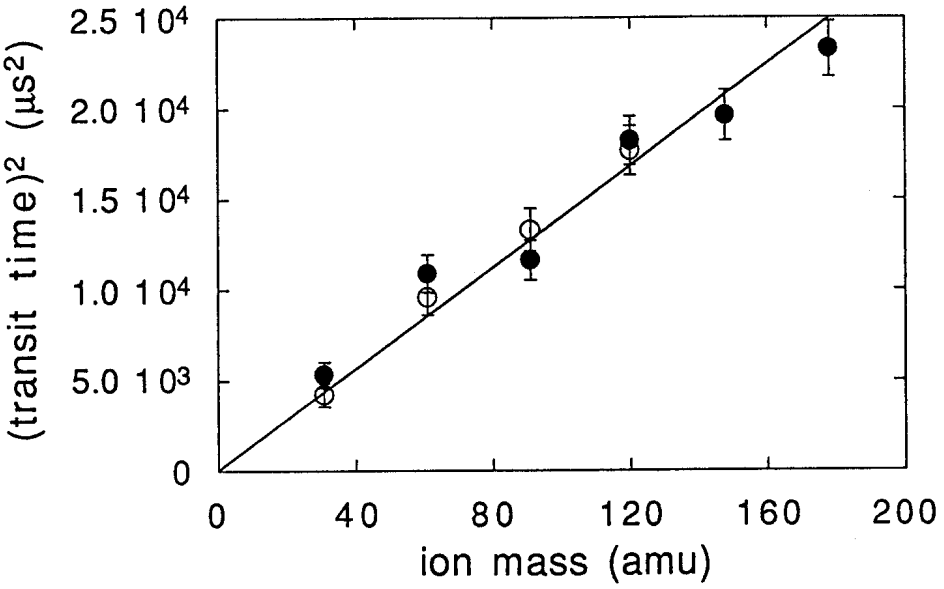

Figure 2 of 15
A A Howling et al
"Time-resolved..."

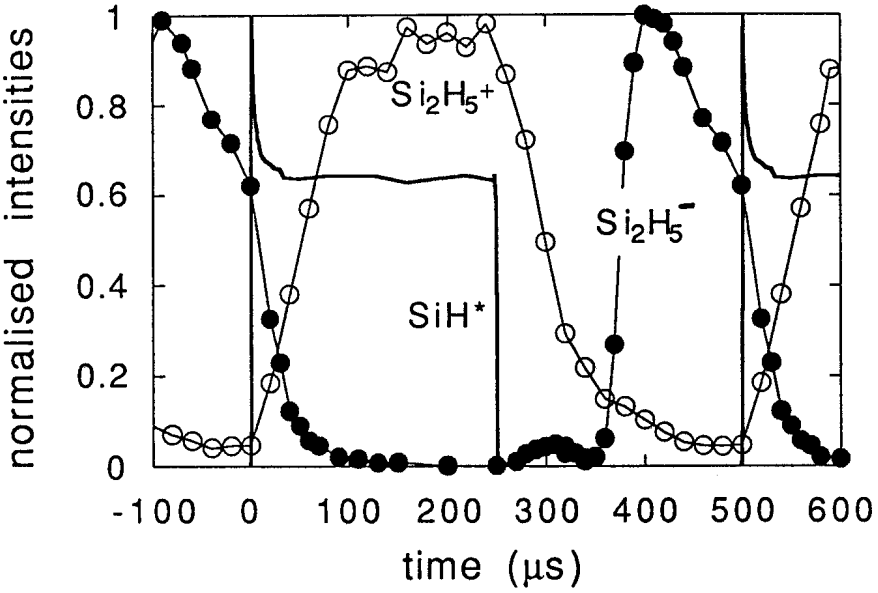

Figure 3 of 15
A A Howling et al
"Time-resolved..."

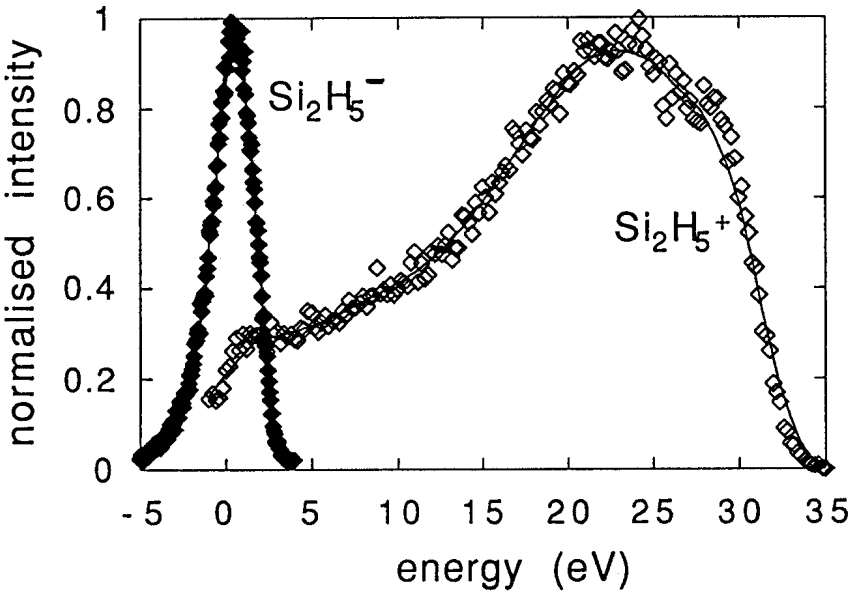

Figure 4 of 15
A A Howling et al
"Time-resolved..."

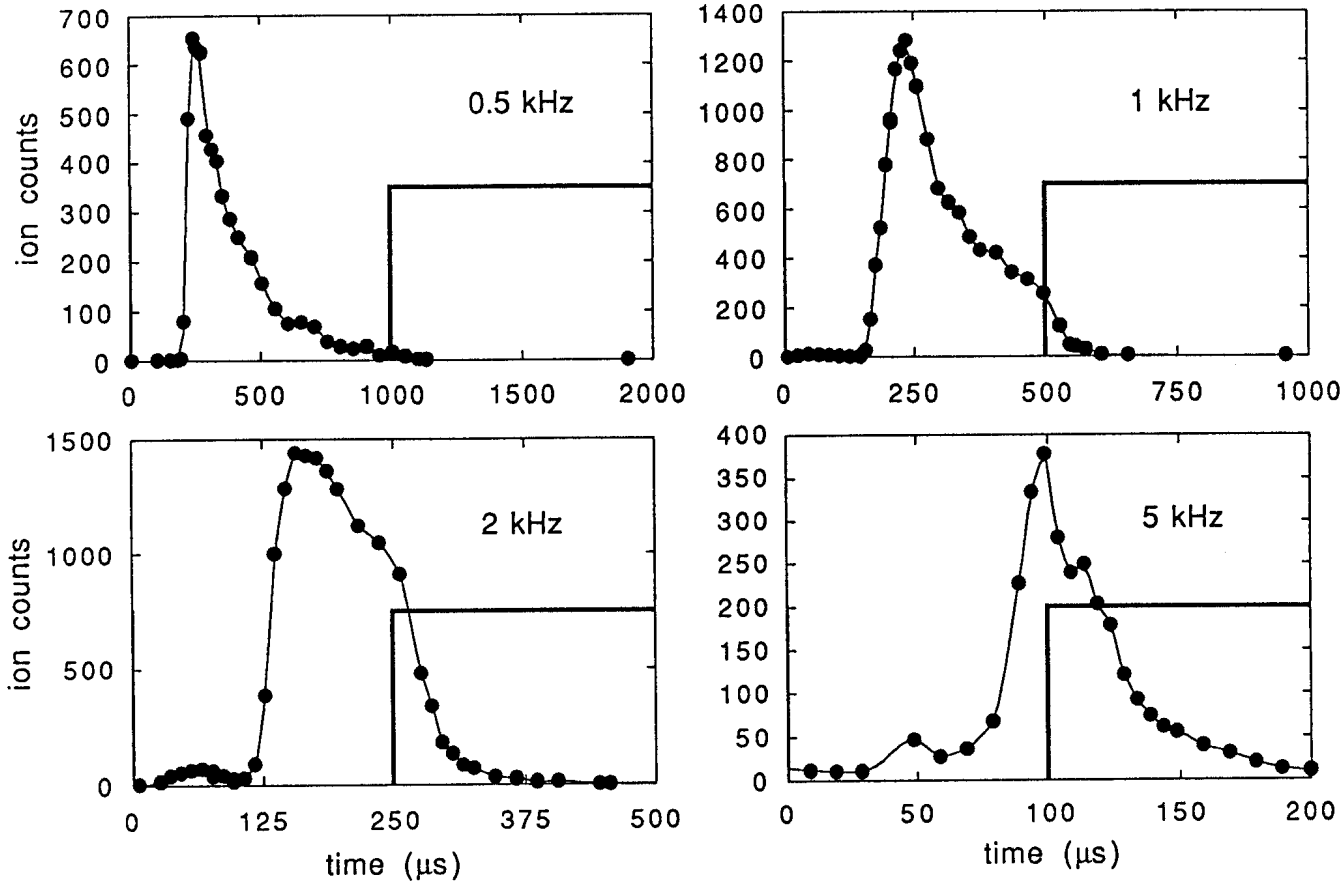

Figure 5 of 15
A A Howling et al
"Time-resolved..."

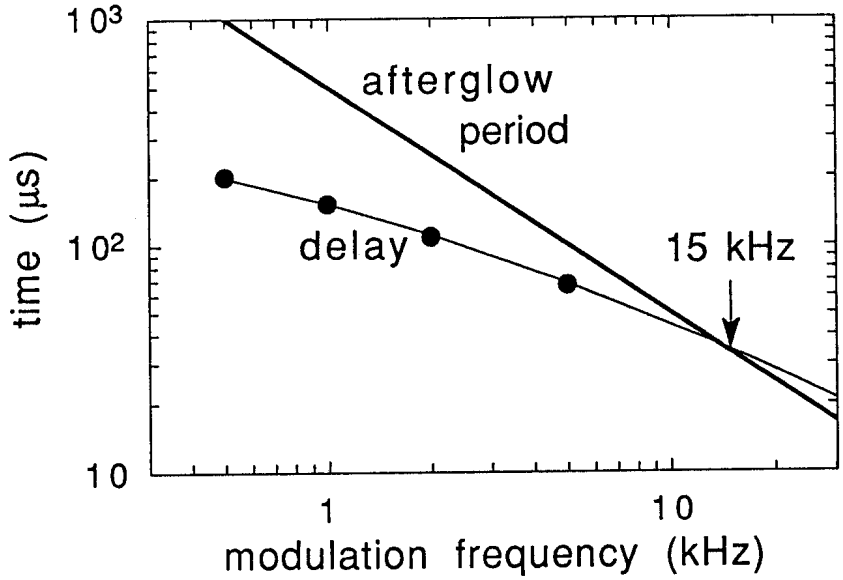

Figure 6 of 15
A A Howling et al
"Time-resolved..."

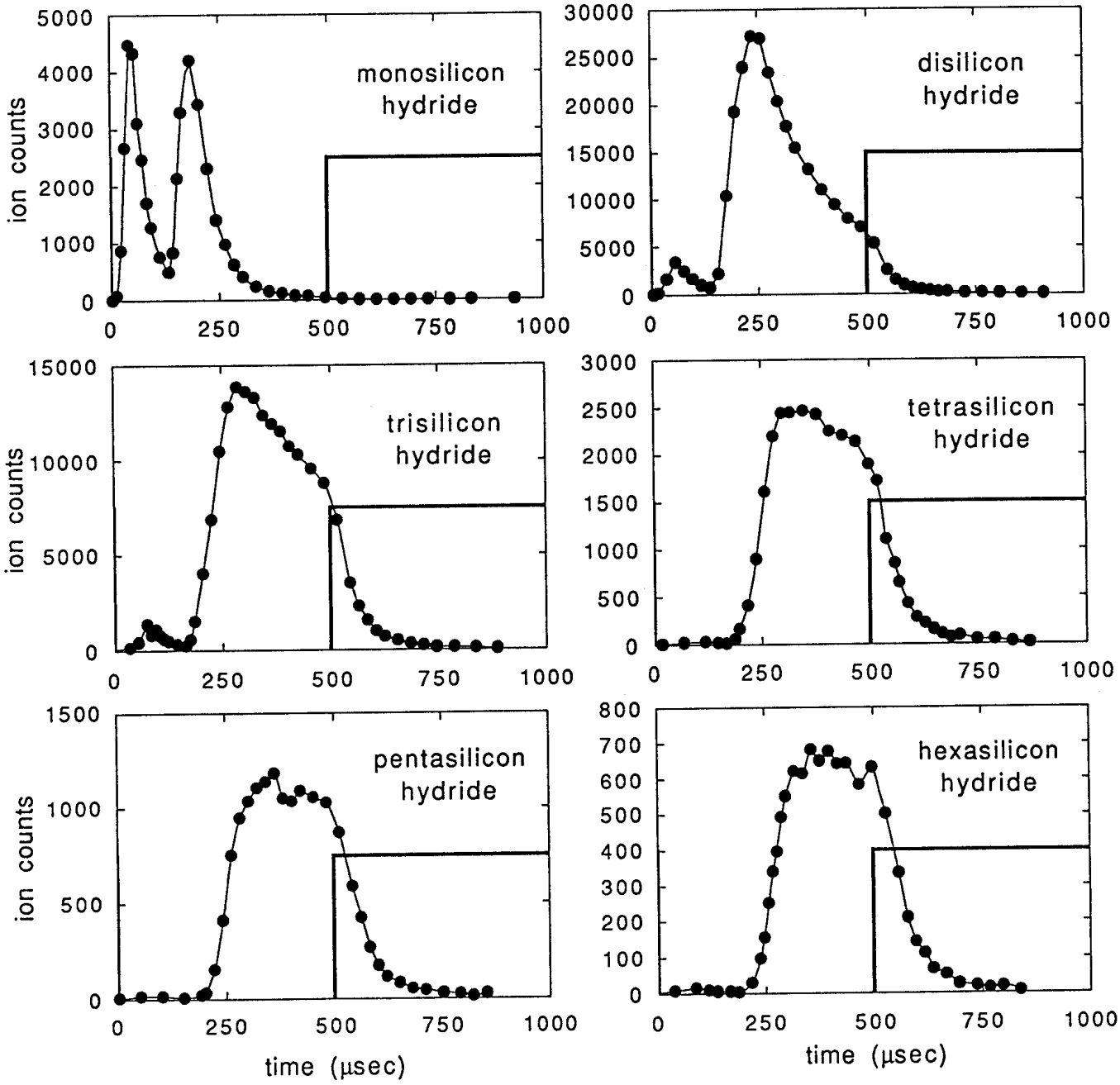

Figure 7 of 15
A A Howling et al
"Time-resolved..."

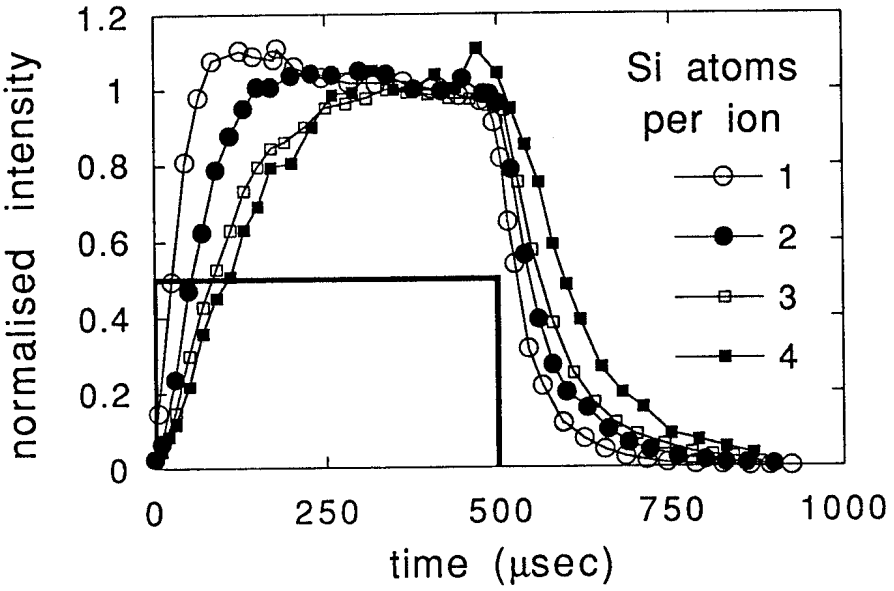

Figure 8 of 15
A A Howling et al
"Time-resolved..."

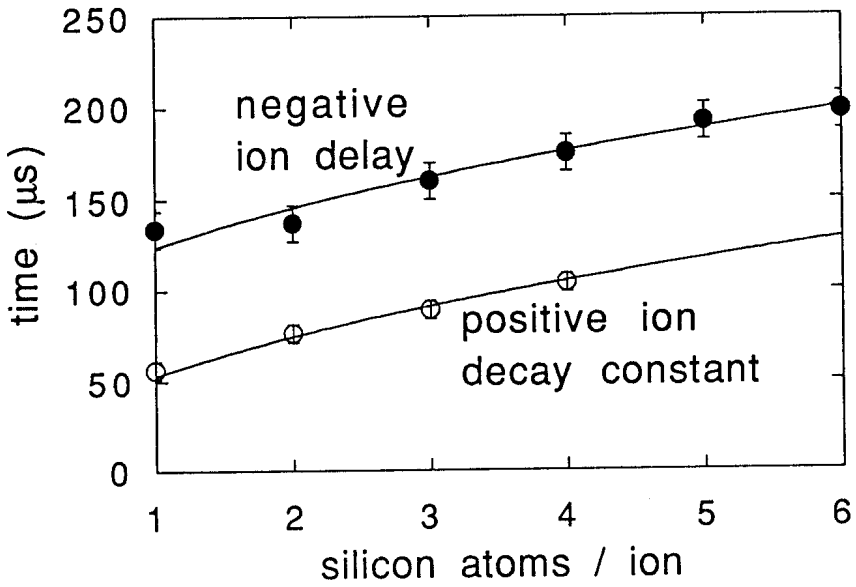

Figure 9 of 15
A A Howling et al
"Time-resolved..."

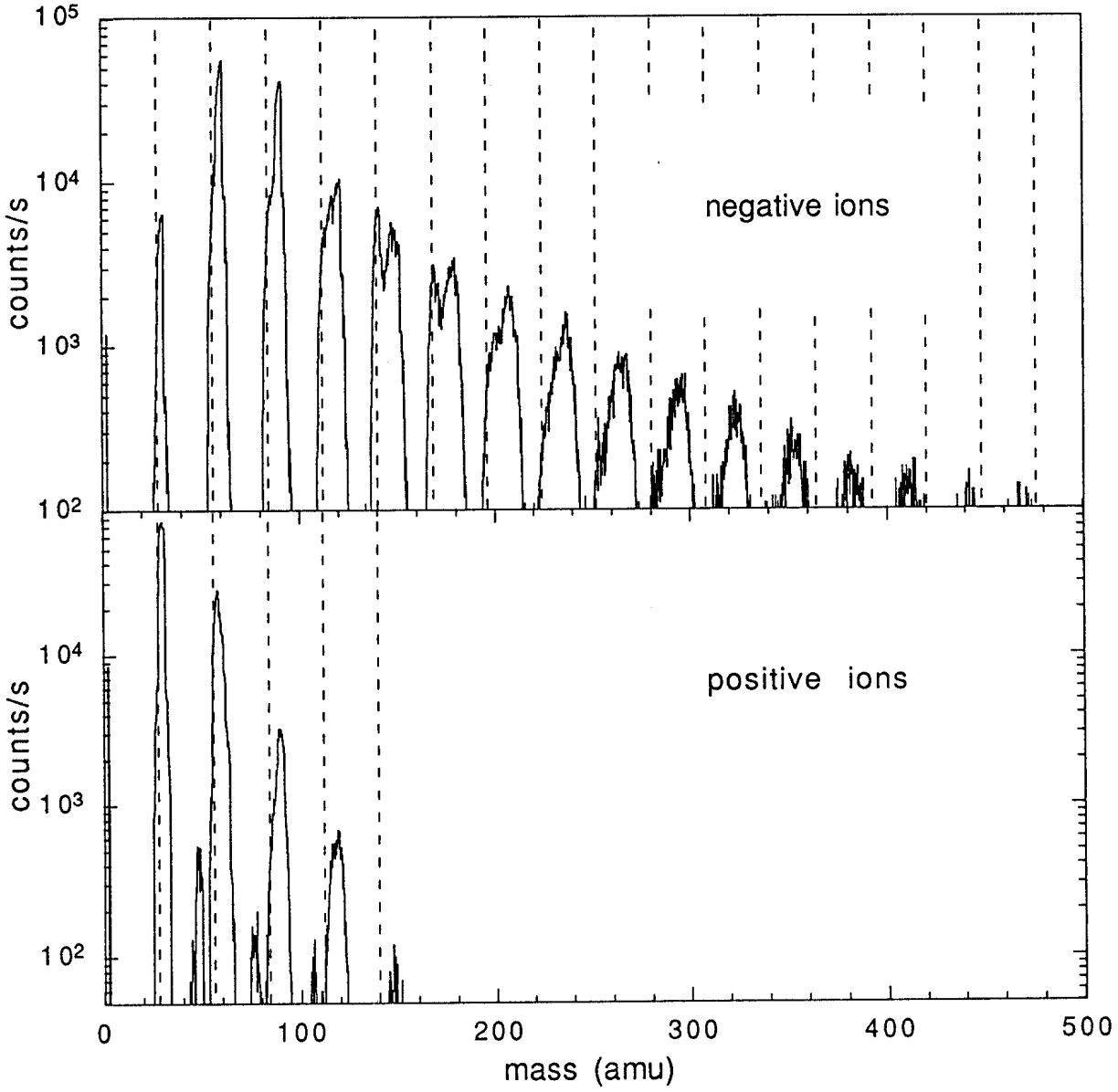

Figure 10 of 15
A A Howling et al
"Time-resolved..."

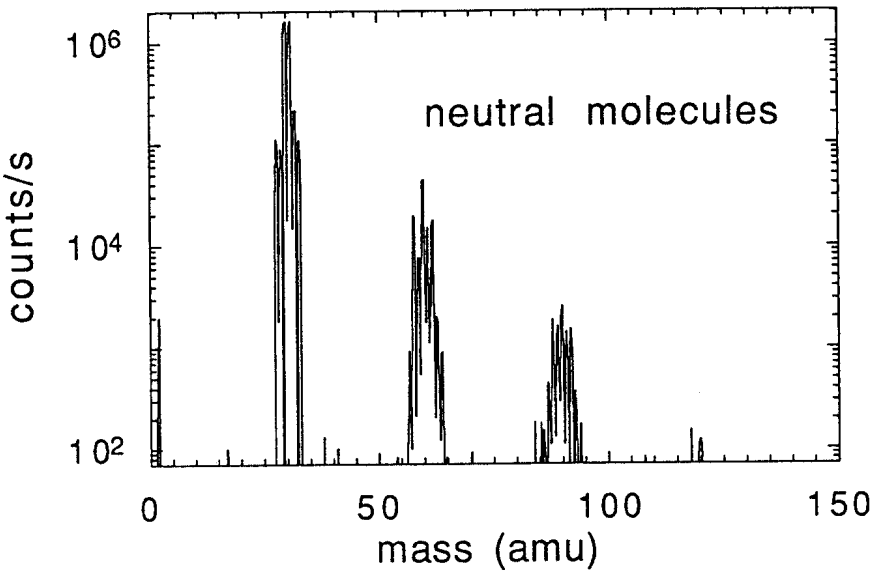

Figure 11 of 15
A A Howling et al
"Time-resolved..."

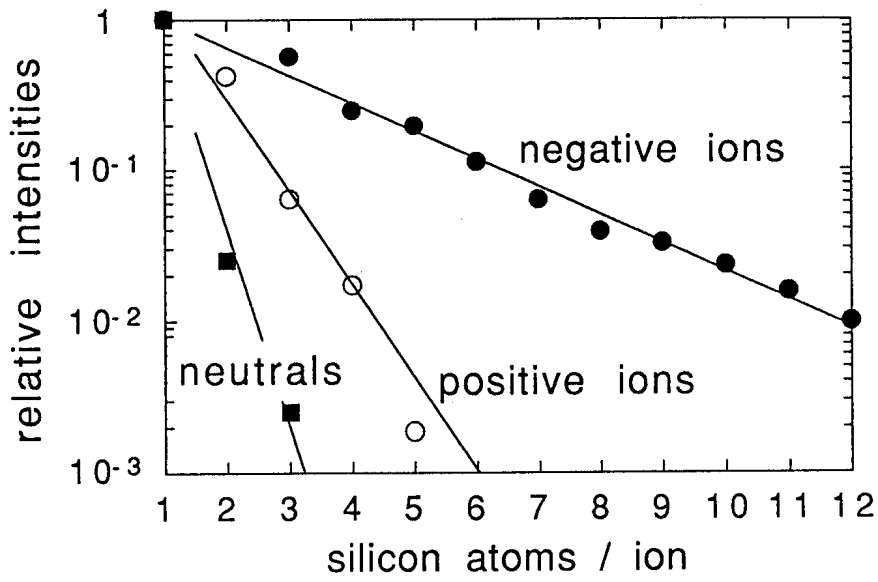

Figure 12 of 15
A A Howling et al
"Time-resolved..."

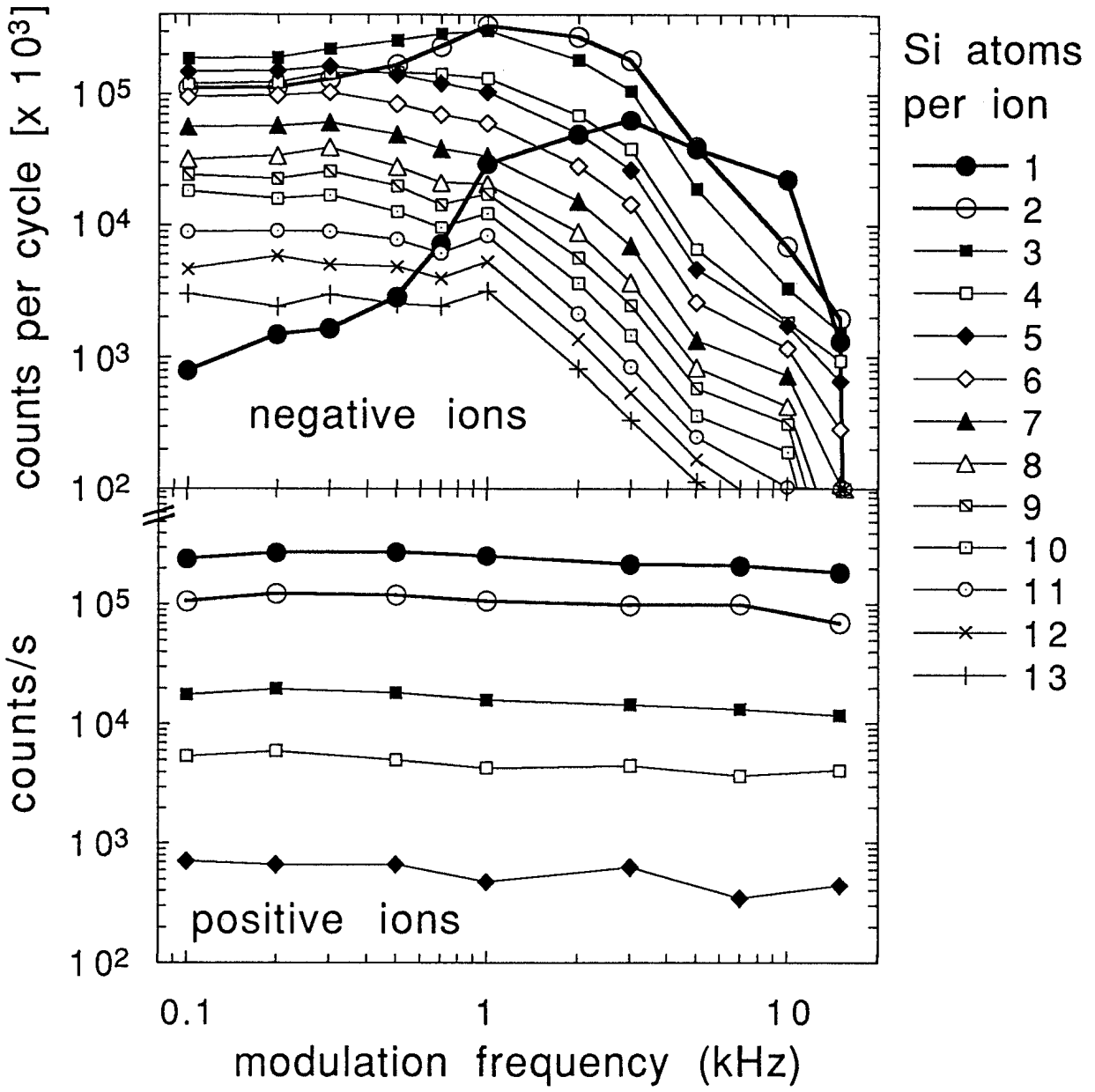

Figure 13 of 15
A A Howling et al
"Time-resolved..."

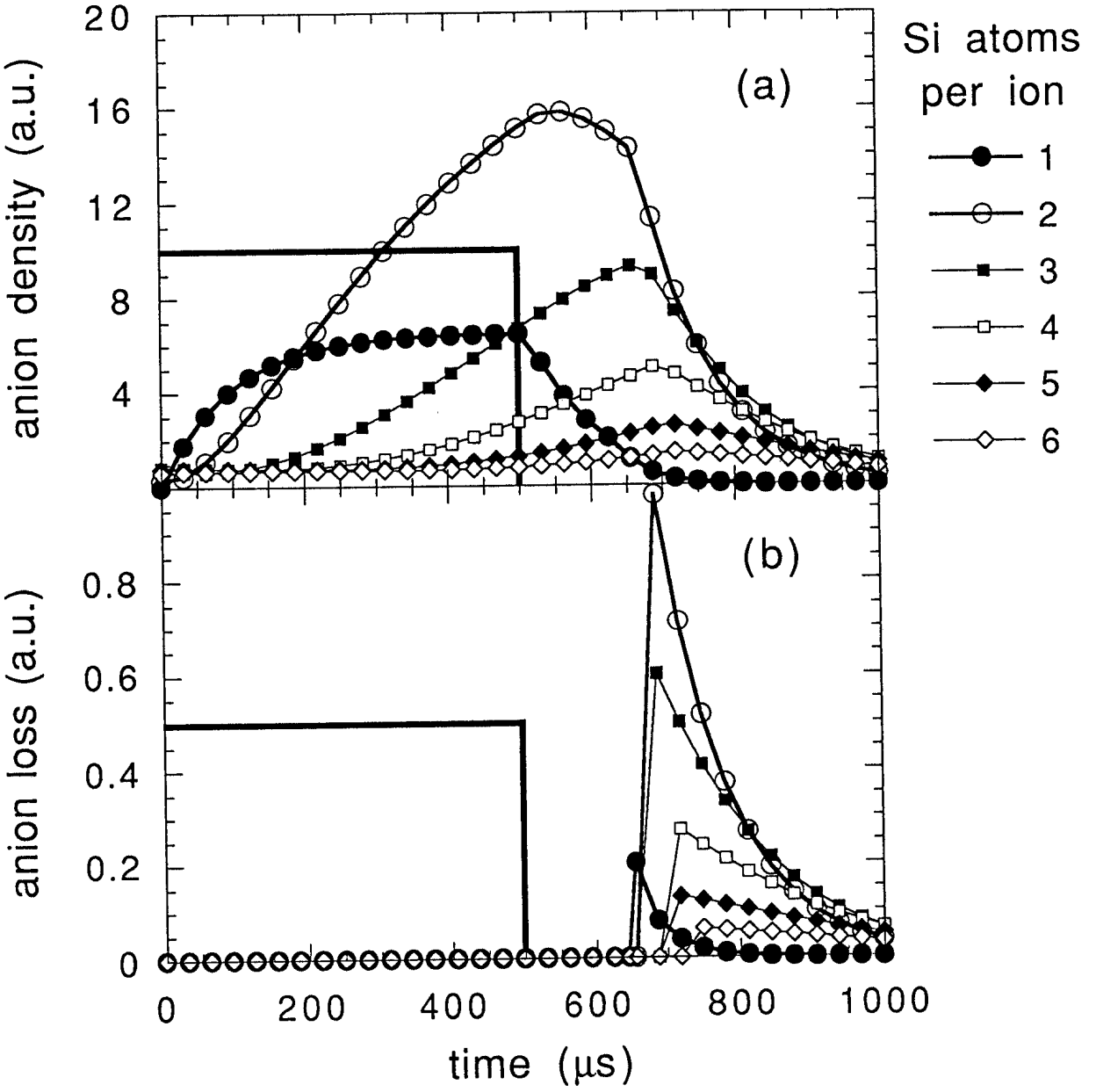

Figure 14 of 15
A A Howling et al
"Time-resolved..."

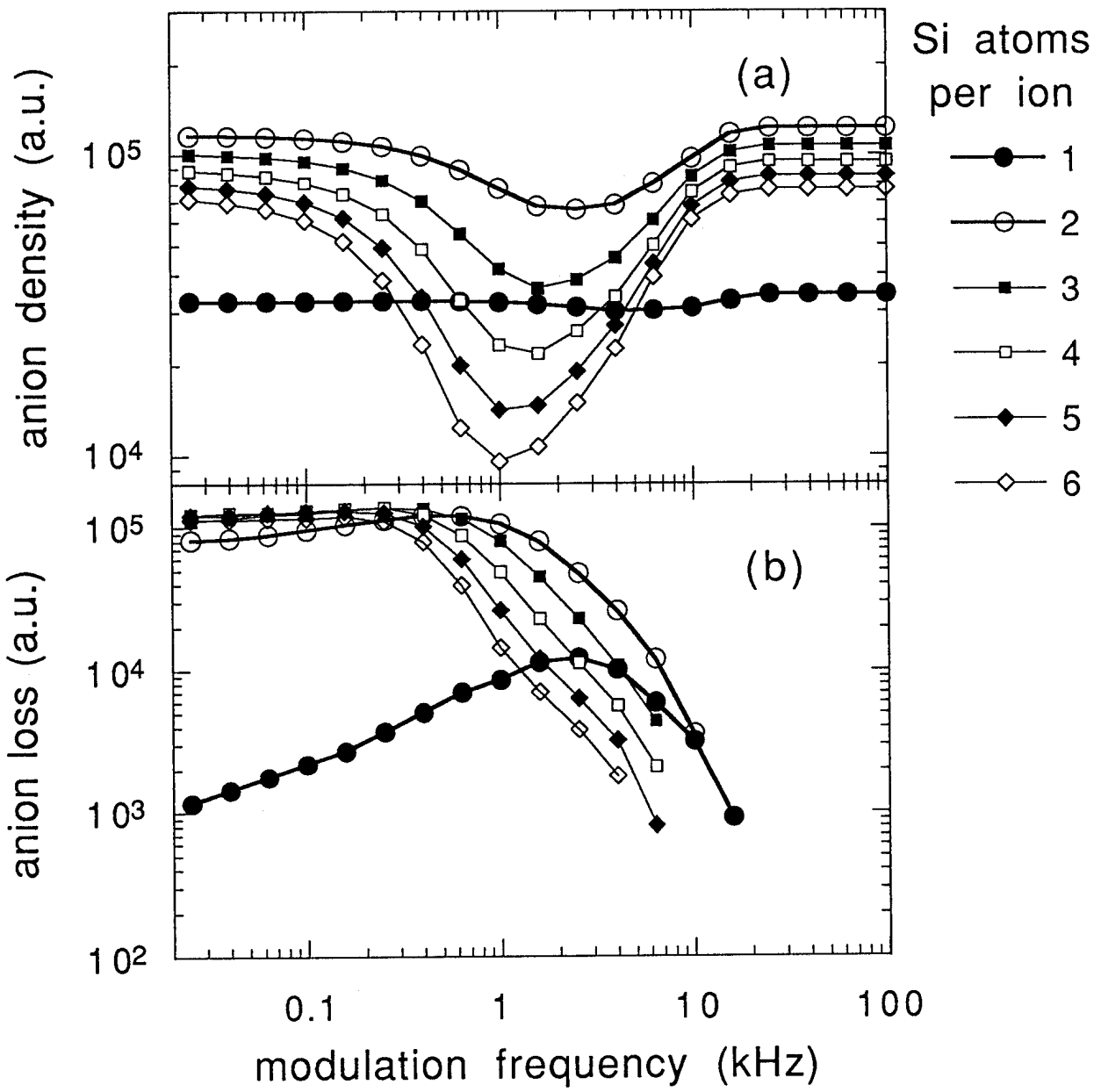

Figure 15 of 15
A A Howling et al
"Time-resolved..."